3

Aerodynamics of Wind Turbines

3.1 General Overview

Wind turbine power production depends on the interaction between the rotor and the wind. As discussed in Chapter 2, the wind may be considered to be a combination of the mean wind and turbulent fluctuations about that mean flow. Experience has shown that the major aspects of wind turbine performance (mean power output and mean loads) are determined by the aerodynamic forces generated by the mean wind. Periodic aerodynamic forces caused by wind shear, off-axis winds and rotor rotation and randomly fluctuating forces induced by turbulence and dynamic effects are the source of fatigue loads and are a factor in the peak loads experienced by a wind turbine. These are, of course, important, but can only be understood once the aerodynamics of steady state operation have been understood. Accordingly, this chapter focuses primarily on steady state aerodynamics. An overview of the complex phenomena of unsteady aerodynamics is presented at the end of the chapter.

Practical horizontal axis wind turbine designs use airfoils to transform the kinetic energy in the wind into useful energy. The material in this chapter provides the background to enable the reader to understand power production with the use of airfoils, to calculate an optimum blade shape for the start of a blade design and to analyse the aerodynamic performance of a rotor with a known blade shape and airfoil characteristics. A number of authors have derived methods for predicting the steady state performance of wind turbine rotors. The classical analysis of the wind turbine was originally developed by Betz and Glauert (Glauert, 1935) in the 1930's. Subsequently, the theory was expanded and adapted for solution by digital computers (see Wilson and Lissaman, 1974, Wilson et al., 1976 and de Vries, 1979). In all of these methods, momentum theory and blade element theory are combined into a strip theory that enables calculation of the performance characteristics of an annular section of the rotor. The characteristics for the entire rotor are then obtained by integrating, or summing, the values obtained for each of the annular sections. This approach is the one used in this chapter.

The chapter starts with the analysis of an idealized wind turbine rotor. The discussion introduces important concepts and illustrates the general behavior of wind turbine rotors and the airflow around wind turbine rotors. The analyses are also used to determine theoretical performance limits for wind turbines.

General aerodynamic concepts and the operation of airfoils are then introduced. This information is then used to consider the advantages of using airfoils for power production over other approaches.

The majority of the chapter details the classical analytical approach for the analysis of horizontal axis wind turbines, as well as some applications and examples of its use. First the details of momentum theory and blade element theory are developed and used to calculate the optimum blade shape for simplified, ideal operating conditions. The results illustrate the derivation of the general blade shape used in wind turbines. The combination of the two approaches, called strip theory or blade element momentum (BEM) theory, is then used to outline a procedure for the aerodynamic design and performance analysis of a wind turbine rotor. Aerodynamic losses and off-design performance are discussed and a starting optimum blade design for a more realistic flow field is developed. Finally, a simplified design procedure is presented that can be used for quick analyses.

The last two sections of the chapter discuss limitations on the maximum theoretical performance of a wind turbine and introduce advanced topics. These advanced topics include the effects of non-ideal steady state aerodynamics, turbine wakes and their effects on turbine operation, unsteady aerodynamics, computer codes for analyzing rotor performance and other theoretical approaches to rotor performance analysis.

Every attempt has been made to make the material in this chapter accessible to readers without a fluid dynamics background. Nevertheless, it would be helpful to be familiar with a variety of concepts including Bernoulli's equation, streamlines, control volume analyses and the concepts of laminar and turbulent flow. The material does require an understanding of basic physics.

3.2 One-Dimensional Momentum Theory and the Betz Limit

A simple model, generally attributed to Betz (1926), can be used to determine the power from an ideal turbine rotor, the thrust of the wind on the ideal rotor and the effect of the rotor operation on the local wind field. This simple model is based on a linear momentum theory developed over 100 years ago to predict the performance of ship propellers.

The analysis assumes a control volume, in which the control volume boundaries are the surface of a stream tube and two cross-sections of the stream tube (see Figure 3.1). The only flow is across the ends of the stream tube. The turbine is represented by a uniform "actuator disk" which creates a discontinuity of pressure in the stream tube of air flowing through it. Note that this analysis is not limited to any particular type of wind turbine.

This analysis uses the following assumptions:

- Homogenous, incompressible, steady state fluid flow
- No frictional drag
- An infinite number of blades
- Uniform thrust over the disk or rotor area
- A nonrotating wake
- The static pressure far upstream and far downstream of the rotor is equal to the undisturbed ambient static pressure

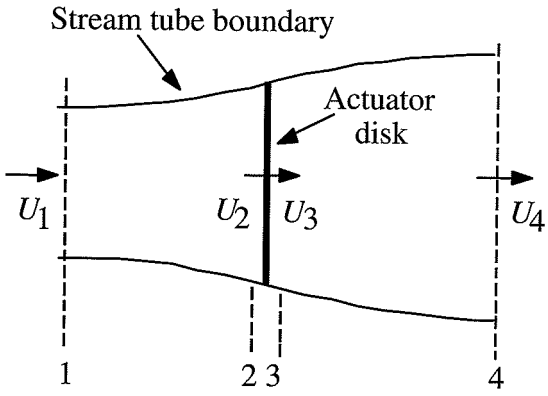

Figure 3.1 Actuator disk model of a wind turbine; U , mean air velocity; 1, 2, 3 and 4 indicate locations

Applying the conservation of linear momentum to the control volume enclosing the whole system, one can find the net force on the contents of the control volume. That force is equal and opposite to the thrust, T, which is the force of the wind on the wind turbine. From the conservation of linear momentum for a one-dimensional, incompressible, time-invariant flow, the thrust is equal and opposite to the change in momentum of air stream:

$$T = U_1(\rho AU)_1 - U_4(\rho AU)_4 \tag{3.2.1}$$

where ρ is the air density, A is the cross sectional area, U is the air velocity and the subscripts indicate values at numbered cross sections in Figure 3.1.

For steady state flow, $(\rho AU)_1 = (\rho AU)_4 = \dot{m}$, where $\dot{m}$ is the mass flow rate. Therefore:

$$T = \dot{m}(U_1 - U_4) \tag{3.2.2}$$

The thrust is positive so the velocity behind the rotor, U_4, is less than the free stream velocity, U_1. No work is done on either side of the turbine rotor. Thus the Bernoulli function can be used in the two control volumes on either side of the actuator disk. In the stream tube upstream of the disk:

$$p_1 + \tfrac{1}{2}\rho U_1^{\,2} = p_2 + \tfrac{1}{2}\rho U_2^{\,2} \tag{3.2.3}$$

In the stream tube downstream of the disk:

$$p_3 + \tfrac{1}{2}\rho U_3^{\,2} = p_4 + \tfrac{1}{2}\rho U_4^{\,2} \tag{3.2.4}$$

where it is assumed that the far upstream and far downstream pressures are equal ($p_1 = p_4$) and that the velocity across the disk remains the same ($U_2 = U_3$).

The thrust can also be expressed as the net sum of the forces on each side of the actuator disc:

$$T = A_2(p_2 - p_3) \tag{3.2.5}$$

If one solves for ($p_2 - p_3$) using Equations 3.2.3 and 3.2.4 and substitutes that into Equation 3.2.5, one obtains:

$$T = \tfrac{1}{2}\rho A_2\left(U_1^2 - U_4^2\right) \tag{3.2.6}$$

Equating the thrust values from Equations 3.2.2 and 3.2.6 and recognizing that the mass flow rate is A_2U_2 , one obtains:

$$U_2 = \frac{U_1 + U_4}{2} \tag{3.2.7}$$

Thus, the wind velocity at the rotor plane, using this simple model, is the average of the upstream and downstream wind speeds.

If one defines the axial induction factor, a , as the fractional decrease in wind velocity between the free stream and the rotor plane, then

$$a = \frac{U_1 - U_2}{U_1} \tag{3.2.8}$$

$$U_2 = U_1(1-a) \tag{3.2.9}$$

and

$$U_4 = U_1(1-2a) \tag{3.2.10}$$

The quantity, U_1a , is often referred to as the induced velocity at the rotor, in which case velocity of the wind at the rotor is a combination of the free stream velocity and the induced wind velocity. As the axial induction factor increases from 0, the wind speed behind the rotor slows more and more. If a = 1/2, the wind has slowed to zero velocity behind the rotor and the simple theory is no longer applicable.

The power out, P , is equal to the thrust times the velocity at the disk:

$$P = \tfrac{1}{2}\rho A_2\left(U_1^2 - U_4^2\right)V_2 = \tfrac{1}{2}\rho A_2U_2(U_1 + U_4)(U_1 - U_4) \tag{3.2.11}$$

Substituting for U_2 and U_4 from Equations 3.2.9 and 3.2.10 gives

$$P = \tfrac{1}{2}\rho A U^3 4a(1-a)^2 \tag{3.2.12}$$

where the control volume area at the rotor, A_2, is replaced with A, the rotor area, and the free stream velocity U_1 is replaced by U.

Wind turbine rotor performance is usually characterized by its power coefficient, C_P:

$$C_P = \frac{P}{\tfrac{1}{2}\rho U^3 A} = \frac{\text{Rotor power}}{\text{Power in the wind}} \tag{3.2.13}$$

The non-dimensional power coefficient represents the fraction of the power in the wind that is extracted by the rotor. From Equation 3.2.12, the power coefficient is:

$$C_P = 4a(1-a)^2 \tag{3.2.14}$$

The maximum C_P is determined by taking the derivative of the power coefficient (Equation 3.2.14) with respect to a and setting it equal to zero, yielding a = 1/3. Thus:

$$C_{P,\max} = 16/27 = 0.5926 \tag{3.2.15}$$

when a = 1/3. For this case, the flow through the disk corresponds to a stream tube with an upstream cross-sectional area of 2/3 the disk area that expands to twice the disk area downstream. This result indicates that, if an ideal rotor were designed and operated such that the wind speed at the rotor were 2/3 of the free stream wind speed, then it would be operating at the point of maximum power production. Furthermore, given the basic laws of physics, this is the maximum power possible.

From Equations 3.2.6, 3.2.9 and 3.2.10, the axial thrust on the disk is:

$$T = \tfrac{1}{2}\rho A U_1^2 [4a(1-a)] \tag{3.2.16}$$

Similarly to the power, the thrust on a wind turbine can be characterized by a non-dimensional thrust coefficient:

$$C_T = \frac{T}{\tfrac{1}{2}\rho U^2 A} = \frac{\text{Thrust force}}{\text{Dynamic force}} \tag{3.2.17}$$

From Equation 3.2.16, the thrust coefficient for an ideal wind turbine is equal to $4a(1-a)$. C_T has a maximum of 1.0 when a = 0.5 and the downstream velocity is zero. At maximum power output (a = 1/3), C_T has a value of 8/9. A graph of the power and thrust coefficients for an ideal Betz turbine and the non-dimensionalized downstream wind speed are illustrated in Figure 3.2.

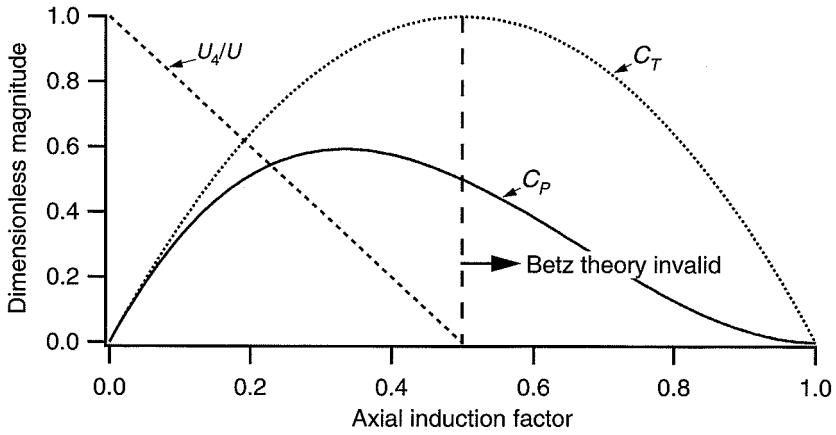

Figure 3.2 Operating parameters for a Betz turbine; U, velocity of undisturbed air; U_4, air velocity behind the rotor,; C_P, power coefficient; C_T, thrust coefficient

As mentioned above, this idealized model is not valid for axial induction factors greater than 0.5. In practice (Wilson et al., 1976), as the axial induction factor approaches and exceeds 0.5, complicated flow patterns that are not represented in this simple model result in thrust coefficients that can go as high as 2.0. The details of wind turbine operation at these high axial induction factors appear in Section 3.7.

The Betz limit, $C_{P,\max} = 16/27$, is the maximum theoretically possible rotor power coefficient. In practice three effects lead to a decrease in the maximum achievable power coefficient:

- Rotation of the wake behind the rotor
- Finite number of blades and associated tip losses
- Non-zero aerodynamic drag

Note that the overall turbine efficiency is a function of both the rotor power coefficient and the mechanical (including electrical) efficiency of the wind turbine:

$$\eta_{overall} = \frac{P_{out}}{\frac{1}{2}\rho A U^3} = \eta_{mech} C_p \tag{3.2.18}$$

Thus:

$$P_{out} = \tfrac{1}{2}\rho A U^3 (\eta_{mech} C_P) \tag{3.2.19}$$

3.3 Ideal Horizontal Axis Wind Turbine with Wake Rotation

In the previous analysis using linear momentum theory, it was assumed that no rotation was imparted to the flow. The previous analysis can be extended to the case where the rotating rotor generates angular momentum, which can be related to rotor torque. In the case of a rotating wind turbine rotor, the flow behind the rotor rotates in the opposite direction to the rotor, in reaction to the torque exerted by the flow on the rotor. An annular stream tube model of this flow, illustrating the rotation of the wake, is shown in Figure 3.3.

The generation of rotational kinetic energy in the wake results in less energy extraction by the rotor than would be expected without wake rotation. In general, the extra kinetic energy in the wind turbine wake will be higher if the generated torque is higher. Thus, as will be shown here, slow running wind turbines (with a low rotational speed and a high torque) experience more wake rotation losses than high-speed wind machines with low torque.

Figure 3.4 gives a schematic of the parameters involved in this analysis. Subscripts denote values at the cross sections identified by numbers. If it is assumed that the angular velocity imparted to the flow stream, ω, is small compared to the angular velocity, Ω, of the wind turbine rotor, then it can also be assumed that the pressure in the far wake is equal to the pressure in the free stream (see Wilson et al., 1976). The analysis that follows is based on the use of an annular stream tube with a radius r and a thickness $\mathrm{d}r$, resulting in a cross-sectional area equal to $2\pi r\mathrm{d}r$ (see Figure 3.4). The pressure, wake rotation and induction factors are all assumed to be a function of radius.

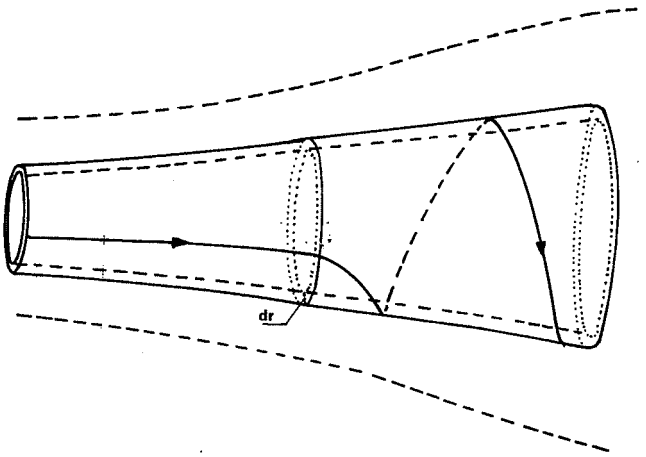

Figure 3.3 Stream tube model of flow behind rotating wind turbine blade. Picture of stream tube with wake rotation, from *Introduction to Wind Energy*, by E. H. Lysen, published by SWD (Steering Committee Wind Energy Developing Countries), Amersfoort, the Netherlands, 1982. Reproduced by permission of the author.

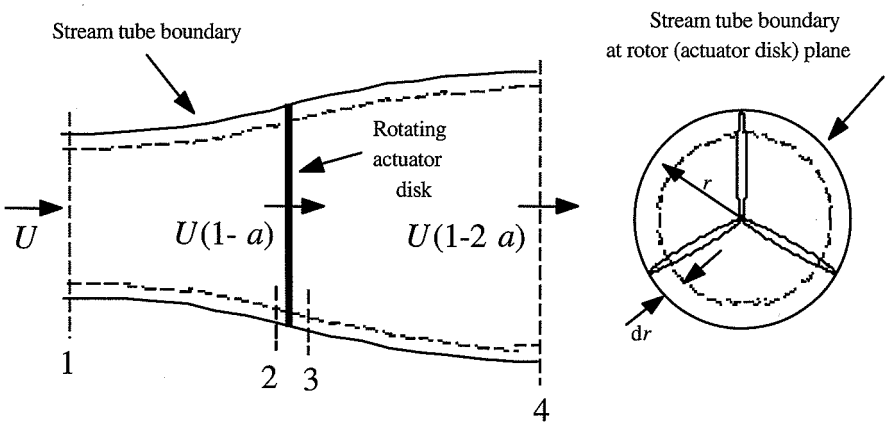

Figure 3.4 Geometry for rotor analysis; U, velocity of undisturbed air; a, induction factor; r, radius

If one uses a control volume that moves with the angular velocity of the blades, the energy equation can be applied in the sections before and after the blades to derive an expression for the pressure difference across the blades (see Glauert, 1935, for the derivation). Note that across the flow disk, the angular velocity of the air relative to the blade increases from Ω to $\Omega+\omega$, while the axial component of the velocity remains constant. The results are:

$$p_2 - p_3 = \rho(\Omega + \tfrac{1}{2}\omega)\omega r^2 \tag{3.3.1}$$

The resulting thrust on an annular element, $\mathrm{d}T$, is:

$$\mathrm{d}T = (p_2 - p_3)\mathrm{d}A = \left[\rho(\Omega + \tfrac{1}{2}\omega)\omega r^2\right] 2\pi r \mathrm{d}r \tag{3.3.2}$$

The angular induction factor, a', is defined as:

$$a' = \omega / 2\Omega \tag{3.3.3}$$

Note that when wake rotation is included in the analysis, the induced velocity at the rotor consists of not only the axial component, Ua, but also a component in the rotor plane, $r\Omega a'$.

The expression for the thrust becomes:

$$\mathrm{d}T = 4a'(1+a')\tfrac{1}{2}\rho\Omega^2 r^2 2\pi r \mathrm{d}r \tag{3.3.4}$$

Following the previous linear momentum analysis, the thrust on an annular cross-section can also be determined by the following expression that uses the axial induction factor, a, (note that U_1, the free stream velocity, is designated by U in this analysis):

$$dT = 4a(1-a)\tfrac{1}{2}\rho U^2 2\pi r dr \tag{3.3.5}$$

Equating the two expressions for thrust gives:

$$\frac{a(1-a)}{a'(1+a)} = \frac{\Omega^2 r^2}{U^2} = \lambda_r^2 \tag{3.3.6}$$

where λ_r is the local speed ratio (see below). This result will be used later in the analysis.

The tip speed ratio, λ, defined as the ratio of the blade tip speed to the free stream wind speed is given by:

$$\lambda = \Omega R/U \tag{3.3.7}$$

The tip speed ratio often occurs in the aerodynamic equations for the rotor. The local speed ratio is the ratio of the rotor speed at some intermediate radius to the wind speed:

$$\lambda_r = \Omega r/U = \lambda r/R \tag{3.3.8}$$

Next, one can derive an expression for the torque on the rotor by applying the conservation of angular momentum. For this situation, the torque exerted on the rotor, Q, must equal the change in angular momentum of the wake. On an incremental annular area element this gives:

$$dQ = d\dot{m}(\omega r)(r) = (\rho U_2 2\pi r dr)(\omega r)(r) \tag{3.3.9}$$

Since $U_2 = U(1-a)$ and $a' = \omega/2\Omega$, this expression reduces to

$$dQ = 4a'(1-a)\tfrac{1}{2}\rho U\Omega r^2 2\pi r dr \tag{3.3.10}$$

The power generated at each element, dP, is given by:

$$dP = \Omega dQ \tag{3.3.11}$$

Substituting for dQ in this expression and using the definition of the local tip speed ratio, λ_r, (Equation 3.3.9), the expression for the power generated at each element becomes:

$$dP = \tfrac{1}{2}\rho AU^3\left[\frac{8}{\lambda^2}a'(1-a)\lambda_r^3\,d\lambda_r\right] \tag{3.3.12}$$

It can be seen that the power from any annular ring is a function of the axial and angular induction factors and the tip speed ratio. The axial and angular induction factors determine the magnitude and direction of the airflow at the rotor plane. The local speed ratio is a function of the tip speed ratio and radius.

The incremental contribution to the power coefficient, dC_P, from each annular ring is given by:

$$dC_P = \frac{dP}{\tfrac{1}{2}\rho AU^3} \tag{3.3.13}$$

Thus

$$C_P = \frac{8}{\lambda^2}\int_0^{\lambda} a'(1-a)\lambda_r^3\,d\lambda_r \tag{3.3.14}$$

In order to integrate this expression, one needs to relate the variables a, a', and λ_r, (see Glauert 1948, Sengupta and Verma, 1992). Solving Equation 3.3.6 to express a' in terms of a, one gets:

$$a' = -\tfrac{1}{2} + \tfrac{1}{2}\sqrt{\left[1+\frac{4}{\lambda_r^2}a(1-a)\right]} \tag{3.3.15}$$

The aerodynamic conditions for the maximum possible power production occur when the term $a'(1-a)$ in Equation 3.3.14 is at its greatest value. Substituting the value for a' from Equation 3.3.15 into $a'(1-a)$ and setting the derivative with respect to a equal to zero yields:

$$\lambda_r^2 = \frac{(1-a)(4a-1)^2}{1-3a} \tag{3.3.16}$$

This equation defines the axial induction factor for maximum power as a function of the local tip speed ratio in each annular ring. Substituting into Equation 3.3.6, one finds that that, for maximum power in each annular ring:

$$a' = \frac{1-3a}{4a-1} \tag{3.3.17}$$

If Equation 3.3.16 is differentiated with respect to a, one obtains a relationship between $d\lambda_r$ and da at those conditions that result in maximum power production:

$$2\lambda_r d\lambda_r = \left[6(4a-1)(1-2a)^2/(1-3a)^2\right] da \tag{3.3.18}$$

Now, substituting the Equations 3.3.16–3.3.18 into the expression for the power coefficient (Equation 3.3.14) gives:

$$C_{P,\max} = \frac{24}{\lambda^2}\int_{a_1}^{a_2}\left[\frac{(1-a)(1-2a)(1-4a)}{(1-3a)}\right]^2 da \tag{3.3.19}$$

Here the lower limit of integration, a_1, corresponds to axial induction factor for $\lambda_r = 0$ and the upper limit, a_2, corresponds to the axial induction factor at $\lambda_r = \lambda$. Also, from Equation 3.3.16:

$$\lambda^2 = (1-a_2)(1-4a_2)^2/(1-3a_2) \tag{3.3.20}$$

Note that from Equation 3.3.16, $a_1 = 0.25$ gives λ_r a value of zero.

Equation 3.3.20 can be solved for the values of a_2 that correspond to operation at tip speed ratios of interest. Note also from Equation 3.3.20, $a_2 = 1/3$ is the upper limit of the axial induction factor, a, giving an infinitely large tip speed ratio.

The definite integral can be evaluated by changing variables: substituting x for $(1-3a)$ in Equation 3.3.19. The result is (see Eggleston and Stoddard, 1987):

$$C_{P,\max} = \frac{8}{729\lambda^2}\left\{\frac{64}{5}x^5+72x^4+124x^3+38x^2-63x-12\left[\ln(x)\right]-4x^{-1}\right\}_{x=(1-3a_2)}^{x=0.25} \tag{3.3.21}$$

Table 3.1 presents a summary of numerical values for $C_{P,\max}$ as a function of λ, with corresponding values for the axial induction factor at the tip, a_2.

The results of this analysis are graphically represented in Figure 3.5, which also shows the Betz limit of the ideal turbine based on the previous linear momentum analysis. The results show that, the higher the tip speed ratio, the greater the maximum theoretical C_P.

These equations can be used to look at the operation of an ideal wind turbine, assuming wake rotation. For example, Figure 3.6 shows the axial and angular induction factors for a turbine with a tip speed ratio of 7.5. It can be seen that the axial induction factors are close to the ideal of 1/3 until one gets near the hub. Angular induction factors are close to zero in the outer parts of the rotor, but increase significantly near the hub.

Table 3.1 Power coefficient, $C_{P,\max}$, as a function of tip speed ratio, λ; a_2 = axial induction factor when the tip speed ratio equals the local speed ratio

λ	a_2	$C_{P,\max}$
0.5	0.2983	0.289
1.0	0.3170	0.416
1.5	0.3245	0.477
2.0	0.3279	0.511
2.5	0.3297	0.533
5.0	0.3324	0.570
7.5	0.3329	0.581
10.0	0.3330	0.585

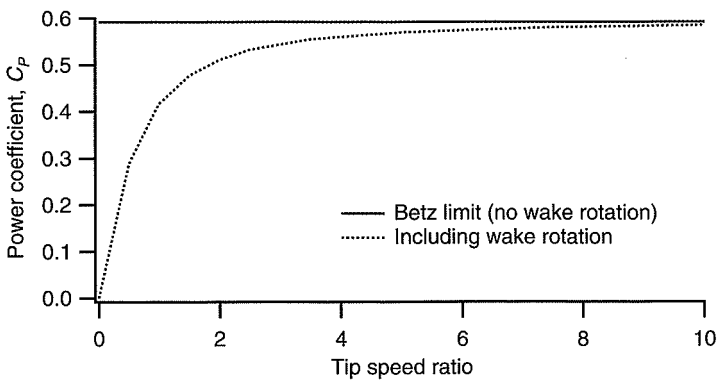

Figure 3.5 Theoretical maximum power coefficient as a function of tip speed ratio for an ideal horizontal axis wind turbine, with and without wake rotation

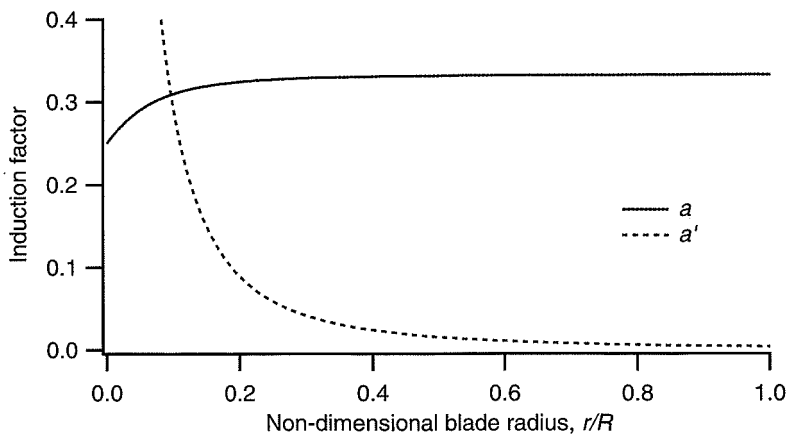

Figure 3.6 Induction factors for an ideal wind turbine with wake rotation; tip speed ratio, $\lambda = 7.5$; a, axial induction factor; a', angular induction factor; r, radius; R rotor radius

In the previous two sections, basic physics has been used to determine the nature of the airflow around a wind turbine and theoretical limits on the maximum power that can be extracted from the wind. The rest of the chapter explains how airfoils can be used to approach this theoretically achievable power extraction.

3.4 Airfoils and General Concepts of Aerodynamics

Wind turbine blades use airfoils to develop mechanical power. The cross-sections of wind turbine blades have the shape of airfoils. The width and length of the blade are functions of the desired aerodynamic performance, the maximum desired rotor power, the assumed airfoil properties and strength considerations. Before the details of wind turbine power production are explained, aerodynamic concepts related to airfoils need to be reviewed.

3.4.1 Airfoil terminology

A number of terms are used to characterize an airfoil, as shown in Figure 3.7. The mean camber line is the locus of points halfway between the upper and lower surfaces of the airfoil. The most forward and rearward points of the mean camber line are on the leading and trailing edges, respectively. The straight line connecting the leading and trailing edges is the chord line of the airfoil, and the distance from the leading to the trailing edge measured along the chord line is designated as the chord, c, of the airfoil. The camber is the distance between the mean camber line and the chord line, measured perpendicular to the chord line. The thickness is the distance between the upper and lower surfaces, also measured perpendicular to the chord line. Finally, the angle of attack, α, is defined as the angle between the relative wind and the chord line. Not shown in the figure is the span of the airfoil, which is the length of the airfoil perpendicular to its cross-section. The geometric parameters that have an effect on the aerodynamic performance of an airfoil include: the leading edge radius, mean camber line, maximum thickness and thickness distribution of the profile and the trailing edge angle.

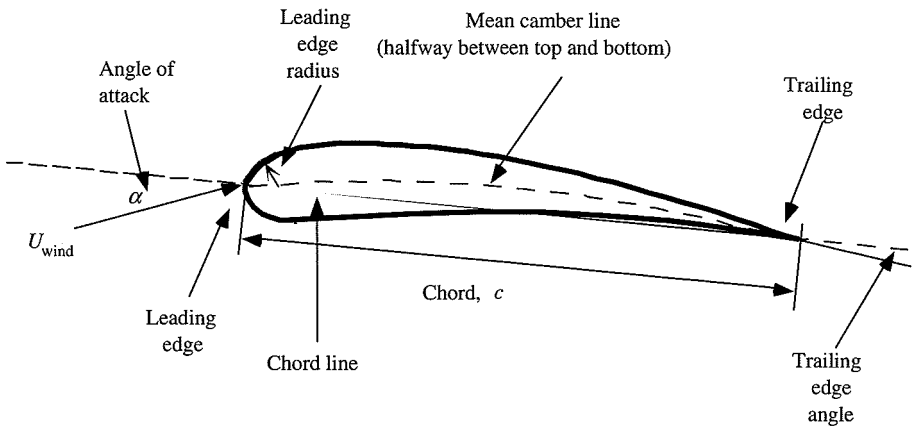

Figure 3.7 Airfoil nomenclature

There are many types of airfoils (see Abbott and Von Doenhoff, 1959, Althaus and Wortmann, 1981, Althaus, 1996, and Tangler, 1987). A few examples of ones that have been used in wind turbine designs are shown in Figure 3.8. The NACA 0012 is a 12% thick symmetric airfoil. The NACA 63(2)-215 is a 15% thick airfoil with a slight camber, and the LS(1)-0417 is a 17% thick airfoil with a larger camber.

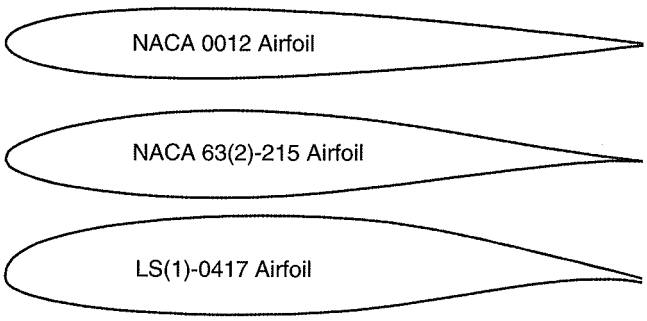

Figure 3.8 Sample airfoils

3.4.2 Lift, drag and non-dimensional parameters

Airflow over an airfoil produces a distribution of forces over the airfoil surface. The flow velocity over airfoils increases over the convex surface resulting in lower average pressure on the 'suction' side of the airfoil compared with the concave or 'pressure' side of the airfoil. Meanwhile, viscous friction between the air and the airfoil surface slows the airflow to some extent next to the surface.

As shown in Figure 3.9, the resultant of all of these pressure and friction forces is usually resolved into two forces and a moment that act along the chord at a distance of $c/4$ from the leading edge (at the 'quarter chord'):

- Lift force – defined to be perpendicular to direction of the oncoming airflow. The lift force is a consequence of the unequal pressure on the upper and lower airfoil surfaces
- Drag force – defined to be parallel to the direction of oncoming airflow. The drag force is due both to viscous friction forces at the surface of the airfoil and to unequal pressure on the airfoil surfaces facing toward and away from the oncoming flow
- Pitching moment – defined to be about an axis perpendicular to the airfoil cross-section

Theory and research have shown that many flow problems can be characterized by non-dimensional parameters. The most important non-dimensional parameter for defining the characteristics of fluid flow conditions is the Reynolds number. The Reynolds number, *Re*, is defined by:

$$Re = \frac{UL}{\nu} = \frac{\rho UL}{\mu} = \frac{\text{Inertial force}}{\text{Viscous force}} \tag{3.4.1}$$

where, ρ is the fluid density, μ is fluid viscosity, $\nu = \mu/\rho$ is the kinematic viscosity and U and L are a velocity and length that characterize the scale of the flow. These might be the free stream velocity and the chord length on an airfoil.

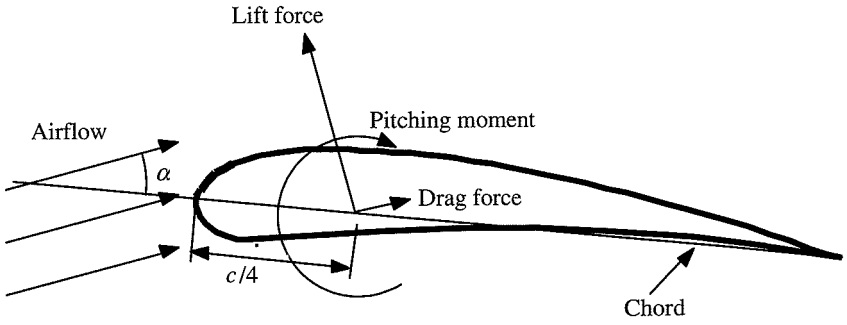

Figure 3.9 Drag and lift forces on stationary airfoil; α, angle of attack; c, chord

Force and moment coefficients, which are a function of Reynolds number, can be defined for two- or three-dimensional objects. Force and moment coefficients for flow around two-dimensional objects are usually designated with a lower case subscript, as in C_d for the two-dimensional drag coefficient. In that case, the forces measured are forces per unit span. Lift and drag coefficients that are measured for flow around three-dimensional objects are usually designated with an upper case subscript, as in C_D. Rotor design usually uses two-dimensional coefficients, determined for a range of angles of attack and Reynolds numbers, in wind tunnel tests. The two-dimensional lift coefficient is defined as:

$$C_l = \frac{L/l}{\frac{1}{2}\rho U^2 c} = \frac{\text{Lift force / unit length}}{\text{Dynamic force / unit length}} \tag{3.4.2}$$

The two-dimensional drag coefficient is defined as:

$$C_d = \frac{D/l}{\frac{1}{2}\rho U^2 c} = \frac{\text{Drag force / unit length}}{\text{Dynamic force / unit length}} \tag{3.4.3}$$

and the pitching moment coefficient is:

$$C_m = \frac{M}{\frac{1}{2}\rho U^2 Ac} = \frac{\text{Pitching moment}}{\text{Dynamic moment}} \tag{3.4.4}$$

where: ρ is the density of air, U is the velocity of undisturbed airflow, A is the projected airfoil area (cord × span), c is the airfoil chord length and l is the airfoil span.

Other dimensionless coefficients that are important for the analysis and design of wind turbines include the power and thrust coefficients and the tip speed ratio, mentioned above, the pressure coefficient, which is used to analyse airfoil flow:

$$C_p = \frac{p - p_\infty}{\frac{1}{2}\rho U^2} = \frac{\text{Static pressure}}{\text{Dynamic pressure}} \tag{3.4.5}$$

and surface roughness ratio:

$$\frac{\varepsilon}{L} = \frac{\text{Surface roughness height}}{\text{Body length}} \tag{3.4.6}$$

3.4.3 *Airfoil behavior*

It is useful to consider the behavior of a symmetric airfoil as a starting point for looking at airfoils for wind turbines. It can be shown (Currie, 1974) that, under ideal conditions, the theoretical lift coefficient of a flat plate is:

$$C_l = 2\pi \sin(\alpha) \tag{3.4.7}$$

and that, under similar ideal conditions, symmetric airfoils of finite thickness have similar theoretical lift coefficients. This would mean that lift coefficients would increase with increasing angles of attack and continue to increase until the angle of attack reaches 90 degrees. The behavior of real symmetric airfoils does indeed approximate this theoretical behavior at low angles of attack. For example, typical lift and drag coefficients for a symmetric airfoil, the NACA 0012 airfoil, the profile of which is shown in Figure 3.8, are shown in Figure 3.10 as a function of angle of attack and Reynolds number. The lift coefficient for a flat plate under ideal conditions is also shown for comparison.

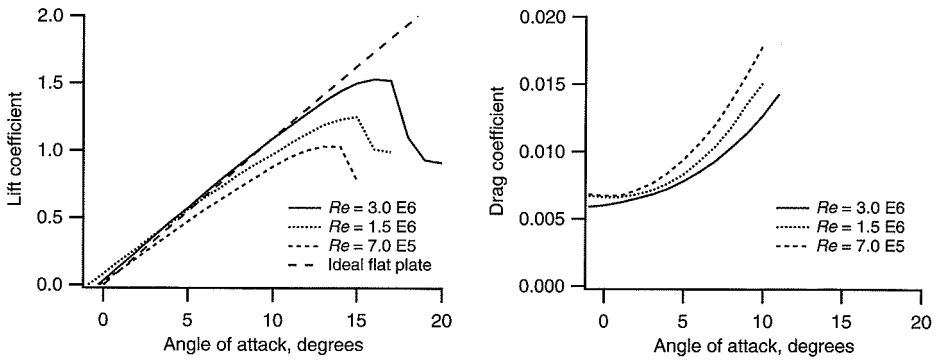

Figure 3.10 Lift and drag coefficients for the NACA 0012 symmetric airfoil (Miley, 1982); *Re*, Reynolds number

Note that, in spite of the very good correlation at low angles of attack, there are significant differences between actual airfoil operation and the theoretical performance at higher angles of attack. The differences are due primarily to the assumption, in the theoretical estimate of the lift coefficient, that air has no viscosity. Surface friction due to viscosity slows the airflow next to the airfoil surface, resulting in a separation of the flow from the surface at higher angles of attack and a rapid decrease in lift. This condition is referred to as stall and is discussed more below.

Airfoils for horizontal axis wind turbines (HAWTs) often are designed to be used at low angles of attack, where lift coefficients are fairly high and drag coefficients are fairly low. The lift coefficient of this symmetric airfoil is about zero at an angle of attack of zero and increases to over 1.0 before decreasing at higher angles of attack. The drag coefficient is usually much lower than the lift coefficient at low angles of attack. It increases at higher angles of attack.

Note, also, that there are significant differences in airfoil behavior at different Reynolds numbers. Rotor designers must make sure that appropriate Reynolds number data are available for the detailed analysis of a wind rotor system.

The lift coefficient at low angles of attack can be increased and drag can often be decreased by using a cambered airfoil (Eggleston and Stoddard, 1987). For example, the DU-93-W-210 airfoil is used in some European wind turbines. Its cross-sectional profile is shown in Figure 3.11. The lift, drag, and pitching moment coefficients for this same airfoil are shown in Figures 3.12 and 3.13 for a Reynolds number of 3 million.

In a manner similar to the behavior of the symmetric airfoil, the lift coefficient for the DU-93-W-210 airfoil increases to about 1.35 but then decreases as the angle of attack increases. Similarly, the drag coefficient starts out very low, but increases at about the same angle of attack that the lift coefficient decreases. This behavior is common to most airfoils. This cambered airfoil also has a nonzero lift coefficient at an angle of attack of zero.

Airfoil behavior can be categorized into three flow regimes: the attached flow regime, the high lift/stall development regime, and the flat plate/fully stalled regime (Spera, 1994). These flow regimes are described below and can be seen in the lift curves above and in Figure 3.14. Figure 3.14 shows the lift and drag coefficients for the S809 airfoil, which has also been used in wind turbines.

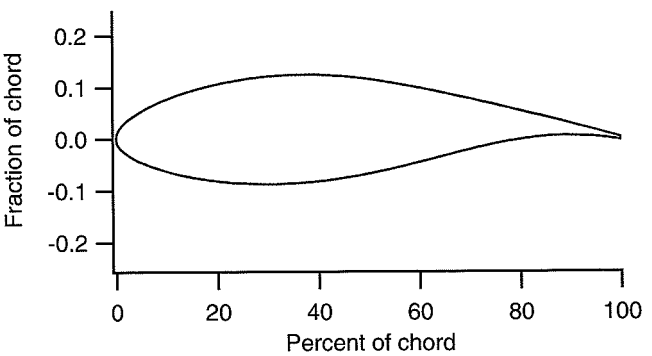

Figure 3.11 DU-93-W-210 airfoil shape

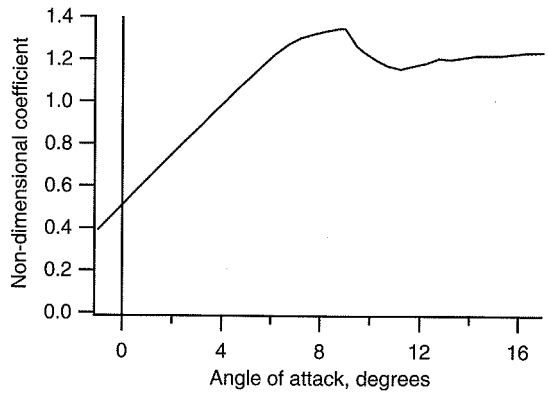

Figure 3.12 Lift coefficients for the DU-93-W-210 airfoil

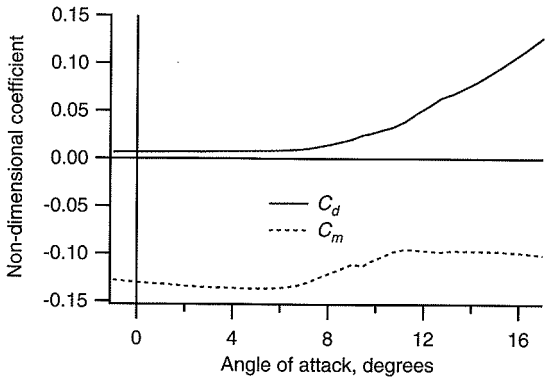

Figure 3.13 Drag and pitching moment coefficients for the DU-93-W-210 airfoil; C_d and C_m, respectively

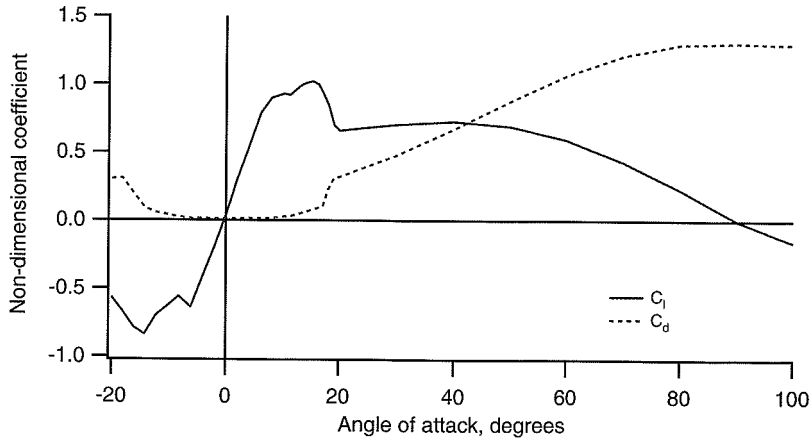

Figure 3.14 Lift and drag coefficients, C_l and C , respectively, for the S809 airfoil; Reynolds Number Re = 75,000,000.

3.4.3.1 Attached flow regime

At low angles of attack (up to about 7 degrees for the DU-93-W-210 airfoil), the flow is attached to the upper surface of the airfoil. In this attached flow regime, lift increases with the angle of attack and drag is relatively low.

3.4.3.2 High lift/stall development regime.

In the high lift/stall development regime (from about 7 to 11 degrees for the DU-93-W-210 airfoil), the lift coefficient peaks as the airfoil becomes increasingly stalled. Stall occurs when the angle of attack exceeds a certain critical value (say 10 to 16 degrees, depending on the Reynolds number) and separation of the boundary layer on the upper surface takes place, as shown in Figure 3.15. This causes a wake to form above the airfoil, which reduces lift and increases drag.

This condition can occur at certain blade locations or conditions of wind turbine operation. It is sometimes used to limit wind turbine power in high winds. For example, many wind turbine designs using fixed pitch blades rely on power regulation control via aerodynamic stall of the blades. That is, as wind speed increases, stall progresses outboard along the span of the blade (toward the tip) causing decreased lift and increased drag. In a well designed, stall regulated machine (see Chapter 7), this results in nearly constant power output as wind speeds increase.

3.4.3.3 Flat plate/fully stalled regime

In the flat plate/fully stalled regime, at larger angles of attack up to 90 degrees, the airfoil acts increasingly like a simple flat plate with approximately equal lift and drag coefficients at an angle of attack of 45 degrees and zero lift at 90 degrees.

3.4.4 Modelling of post-stall airfoil characteristics

Measured wind turbine airfoil data are used to design wind turbine blades. Wind turbine blades may often operate in the stalled region of operation, but data at high angles of attack are sometimes unavailable. Because of the similarity of stalled behavior to flat plate behavior, models have been developed to model lift and drag coefficients for stalled operation. Information on modelling post stall behavior of wind turbine airfoils can be found in Viterna and Corrigan (1981). Summaries of the Viterna and Corrigan model can be found in Spera (1994) and Eggleston and Stoddard (1987).

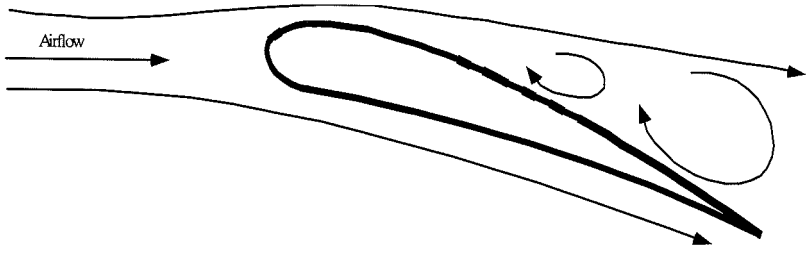

Figure 3.15 Illustration of airfoil stall

3.4.5 *Airfoils for wind turbines*

Modern HAWT blades have been designed using airfoil 'families' (Hansen and Butterfield, 1993). That is, the blade tip is designed using a thin airfoil, for high lift to drag ratio, and the root region is designed using a thick version of the same airfoil for structural support. Typical Reynolds numbers found in wind turbine operation are in the range of 500,000 and 10 million. A catalogue of airfoil data at these 'low' Reynolds numbers was compiled by Miley (1982). Generally, in the 1970s and early 1980s, wind turbine designers felt that minor differences in airfoil performance characteristics were far less important than optimising blade twist and taper. For this reason, little attention was paid to the task of airfoil selection. Thus, airfoils that were in use by the helicopter industry were chosen because the helicopter was viewed as a similar application. Aviation airfoils such as the NACA 44xx and NACA 230xx (Abbott and Von Doenhoff, 1959) were popular airfoil choices because they had high maximum lift coefficients, low pitching moment, and low minimum drag.

The NACA classification has 4, 5, and 6 series wing sections. For wind turbines, 4 digit series are generally used, for example: NACA 4415. The first integer indicates the maximum value of the mean camber line ordinate in percent of the chord. The second integer indicates the distance from the leading edge to maximum camber in tenths of the chord. The last two integers indicate the maximum section thickness in percent of the chord.

In the early 1980s wind turbine designers became aware of airfoils such as the NASA LS(1) MOD, and this airfoil was chosen by U.S. and British designers for its reduced sensitivity to leading edge roughness, compared to the NACA 44xx and NACA 230xx series airfoils (Tangler et al., 1990). Danish wind turbine designers began to use the NACA 63(2)-xx instead of the NACA 44xx airfoils for the same reasons.

The experience gained from operating these traditional airfoils has highlighted the shortcomings of such airfoils for wind turbine applications. Specifically, stall controlled HAWTs commonly produced too much power in high winds. This caused generator damage. Stall controlled turbines were operating with some part of the blade in deep stall for more than 50% of the life of the machine. Peak power and peak blade loads all occurred while the turbine was operating with most of the blade stalled, and predicted loads were only 50% to 70% of the measured loads. Designers began to realize that a better understanding of airfoil stall performance was important. In addition, leading edge roughness affected rotor performance. For example, with the early airfoil designs, when the blades accumulate insects and dirt along the leading edge, power output can drop as much as 40% of its clean value. Even the LS(1) MOD airfoils, which were designed to tolerate surface roughness, experienced a loss of power in the field once blades became soiled.

As a consequence of these experiences, airfoil selection criteria, and the designs for wind turbine airfoils and blades, have had to change to achieve high and reliable performance. New airfoil design codes have been used by wind energy engineers to design airfoils specifically for HAWTs. One of the most used codes in wind energy engineering was developed by Eppler and Somers (1980). This code combines a variety of techniques to optimize boundary layer characteristics and airfoil shapes to achieve specified performance criteria.

Using the Eppler code, researchers at the National Renewable Energy Laboratory (Spera, 1994) have developed 'special purpose families' of airfoils for three different

classes of wind turbines (the SERI designated classification of airfoils). As reported by Tangler et al. (1990) these S-Series airfoils have been tested on 8 m long blades and have been shown to be relatively insensitive to leading edge surface roughness and contributed to increased annual energy production by allowing a larger rotor diameter without increased peak power. These airfoils are now used on some commercial wind turbines.

3.4.6 *Lift versus drag machines*

Wind energy converters that have been built over the centuries can be divided into lift machines and drag machines. Lift machines use lift forces to generate power. Drag machines use drag forces. The horizontal axis wind turbines that are the primary topic of this book (and almost all modern wind turbines) are lift machines, but many useful drag machines have been developed. The advantages of lift over drag machines are described in this section through the use of a few simple examples.

A simple drag machine, shown in Figure 3.16, was used in the Middle East over a thousand years ago (Gasch, 1996). It includes a vertical axis rotor consisting of flat surfaces in which half of the rotor is shielded from the wind. The simplified model on the right in Figure 3.16 is used to analyse the performance of this drag machine.

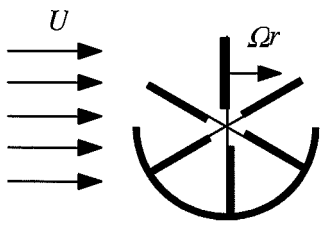

Drag machine

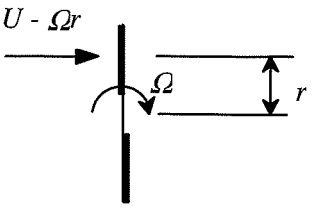

Drag machine model

Figure 3.16 Simple drag machine and model; U, velocity of the undisturbed airflow; Ω, angular velocity of wind turbine rotor; r, radius

The drag force, F_D, is a function of the relative wind velocity at the rotor surface (the difference between the wind speed, U, and the speed of the surface is Ωr):

$$F_D = C_D\left[\tfrac{1}{2}\rho(U-\Omega r)^2 A\right] \tag{3.4.8}$$

where A is the drag surface area and where the three-dimensional drag coefficient, C_D, for a square plate is assumed to be 1.1.

The rotor power is the product of the drag force and rotational speed of the rotor surfaces:

$$P = C_D\left[\tfrac{1}{2}\rho A(U-\Omega r)^2\right]\Omega r = \left(\rho A U^3\right)\left[\tfrac{1}{2}C_D\lambda(1-\lambda)^2\right] \tag{3.4.9}$$

The power coefficient, shown in Figure 3.17, is a function of λ, the ratio of the surface velocity to the wind speed, and is based on an assumed total machine area of 2A:

$$C_P = \left[\tfrac{1}{2} C_D \lambda (1-\lambda)^2\right] \tag{3.4.10}$$

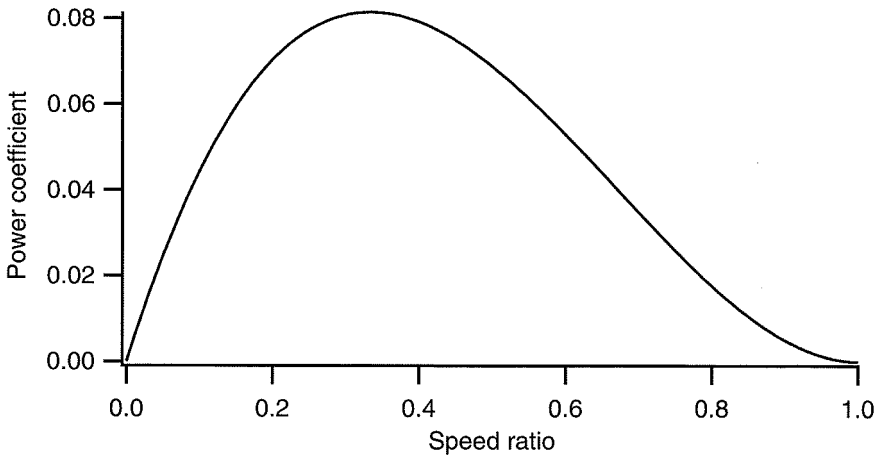

Figure 3.17 Power coefficient of flat plate drag machine

The power coefficient is zero at speed ratios of zero (no motion) and 1.0 (the speed at which the surface moves at the wind speed and experiences no drag force). The peak power coefficient of 0.08 occurs as a speed ratio of 1/3. This power coefficient is significantly lower than the Betz limit of 0.593. This example also illustrates one of the primary disadvantages of a pure drag machine: the rotor surface cannot move faster than the wind speed. Thus, the wind velocity relative to the power producing surfaces of the machine, U_{rel}, is limited to the free stream velocity:

$$U_{rel} = U(1-\lambda) \qquad \lambda < 1 \tag{3.4.11}$$

The forces in lift machines are also a function of the relative wind velocity and of the lift coefficient:

$$F_L = C_L\left(\tfrac{1}{2}\rho A U_{rel}{}^2\right) \tag{3.4.12}$$

The maximum lift and drag coefficients of airfoils are of similar magnitude. One significant difference in the performance between lift and drag machines is the much higher relative wind velocities that can be achieved with lift machines. Relative velocities are always greater than the free stream wind speed, sometimes by an order of magnitude. As illustrated in Figure 3.18, the relative wind velocity at the airfoil of a lift machine is:

$$U_{rel} = \sqrt{U^2 + (\Omega r)^2} = U\sqrt{1+\lambda^2} \tag{3.4.13}$$

With speed ratios of up to 10, and forces that are a function of the square of the relative speed, it can be seen that the forces that can be developed by a lift machine are significantly greater than those achievable with a drag machine with the same surface area. The larger forces allow for much greater power coefficients.

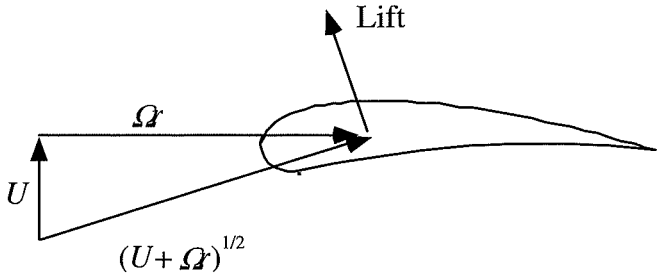

Figure 3.18 Relative velocity of a lift machine; for notation, see Figure 3.16

It should be pointed out that some drag-based machines, such as the Savonius rotor, may achieve maximum power coefficients of greater than 0.2 and may have tip speed ratios greater than 1.0. This is primarily due to the lift developed when the rotor surfaces turn out of the wind as the rotor rotates (Wilson et al., 1976). Thus, the Savonius rotor and many other drag-based devices may also experience some lift forces.